OPTOFLUIDIC DEVICE WITH A MULTIPLE COUPLED GEOMETRIES FOR CANCER CELLS DETECTION FROM RESPIRATORY TRACT USING SALIVA SAMPLES

MASTER'S DEGREE THESIS

Jesus David Coral Pérez

Supervised by Dr. Xavier Mateos and Dr. Rosa Maria Solé

MASTER'S DEGREE IN NANOSCIENCE, MATERIALS AND PROCESSES

UNIVERSITAT ROVIRA I VIRGILI

Tarragona

2020

OPTOFLUIDIC DEVICE WITH A MULTIPLE COUPLED GEOMETRIES FOR CANCER CELLS DETECTION FROM RESPIRATORY TRACT USING SALIVA SAMPLES

Jesus David Coral Pérez
Master Program in Nanoscience, Materials and Processes, 2019-2020
e-mail: jesusdavid.coral@estudiants.urv.cat

Supervisors: Xavier Mateos and Rosa Maria Solé.
Universitat Rovira i Virgili. Physics and Crystallography of Materials and Nanomaterials (FiCMA-FiCNA) group of research.
Marcel.li Domingo 1, 43007 Tarragona Spain

Abstract
The saliva is a secretion which can present Cancer Tumor Cells (CTCs) of cancer patients. Its analysis is a developing field which may be essential for early detection of cancer and monitoring of treatment. Here, we use different connected geometries for mixing, sorting, concentrating and confining fluids and particles inside a fluids. The first two geometries are a mixer-separator assembly, with a Fermat spiral design, followed by a continuous flow concentrator and a serpentine design to align the particles of interest (CTCs). Device performance was optimized using COMSOL Multiphysics software, to works with high pressures inlets (350 mbar for water or serum and 294 mbar for saliva sample) as optimum pressure inlets. The numerical models were corroborated through experimentation using two types of polystyrene (PS) particles of $5\mu m$ and $20\mu m$. The optofluidic device identifies and addresses the next challenges using optical detections: mixing tests including two fluids with similar density, proper particle sorting by size using Dean Flow Fractionation (DFF), and single-step retrieval of labelled large particles.

1 Introduction

In the medical field, it is essential to determine signs and symptoms to diagnose a disease. Likewise, it is sought to detect prevalent diseases long before symptoms appear as a method to prevent diseases in irreversible stages. An example of such methods includes the detection of diseases through genomic analysis. However, this branch of science is still under development, and genomic treatments may not be applied on all occasions. For this reason, when a patient presents a detectable discomfort, the disease may be in an irreversible state due to the lack of a method to prevent it. Therefore, a strategy known as screening has been created whose purpose is to detect a disease in its initial or advanced stages, using a diagnostic method in a population at risk [1]. However, based on Wilson and Jurgen [2], it is necessary to meet specific criteria to be able to run an accurate screening test.

Cancer is a disease caused by various internal or external factors that alter the genetic code of cells. Additionally, cancer is the second cause of death in the world, with 18.1 million diagnosed and 9.6 million deaths present only in 2018 [3–5]. Within this disease, lung cancer represents 11.6% of cancers in the world. Furthermore, it is the main cause of cancer's deaths, with 20% of mortality.

Two million diagnoses of lung cancer were found in 2016, which 1.7 million deaths were associated with lung cancer. This represents a total of 36.4 million DALY's in that year [4, 6]. A DALY describes the sum of years lost due to premature mortality and its relationship with the years of life lived with disability [7]. Due to the arguments above, it is crucial to find an effective method for the early detection of respiratory tract cancer.

Nowadays, one of the most used method is low-dose computed tomography (LDCT). The US Preventive Services Task Force (USA) recommends this method to patients between 55 and 80 years of age who have a smoking history of 30 packets of tobacco per year for more than 30 years [4, 6, 7]. In an experiment conducted by the National Lung Screening Trial (NLST), LDCT has been tested as a preventive method in the early stages (A1) of lung cancer, thus reducing the mortality rate by 6.2% [8]. Applying the screening test on asymptomatic patients with a high probability of developing cancer results in a drastic reduction of mortality. However, this method has a high false-positive rate despite the test optimization efforts by implementing the volumetric criteria [9].

Alternative sources for screening tests reside on testing saliva. Saliva is a human secretion that

can present small concentrations of cancer cells in patients with cancer affectations. The mixture of saliva and serum were analyzed in recent years using Surface Enhanced Raman Spectroscopy with positive results in the detection of breast tumour cells and lung cancer cells [10, 11]. Also, different authors such as Fang Wei et al. [12] are researching with multiplexable electrochemical sensors to identify mutations in the epidermal growth factor receptor (EGFR) to detect non-small cancer lung carcinomas. Hence, it is possible to use microfluidic methods to create a device for detecting cancer cells in the respiratory tract.

Moreover, saliva can be studied in a microfluidic system following the branch of lab on a chip. However, it should also be considered that saliva is a fluid that has minimal concentrations of respiratory tract cells. It also contains proteins, DNA, ARN or microbiotas [13]. These components can make it difficult to detect cancer cells by optical methods in microfluidic systems.

The lab on a chip are microfluidic systems originated in nano- and micrometric scale, usually under 1 μm or micrometric scale between 10 μm to 200 μm[14]. These microfluidic systems are based on the concept of Total Analysis System (TAS), which consists of integrating various steps or processes for chemical analysis in a single device [15–17]. Most microfluidic systems can be classified into three main groups: passive systems, active systems, and manuals. Mainly, the difference between active and passive systems lies in the intrusion of external agents such as temperature, gravity, electric, magnetic or acoustic fields in the microfluidic system to accelerate or facilitate the functionality of the device [18]. In contrast, manual devices work independently of automatic pumping systems or electronic equipment such as the cases of the authors Peter Thurgood and Jiu Yang, who developed a self-sufficient pressure pump using latex balloons[19].

A microfluidic system can facilitate the task of particle and cell detection in a fluid. The lab on a chip branch counts with different operational units to control the physical behaviour of particles in a channel. E.g. Depending of the geometry design, it can perform different unit processes such mixture [20], separation [21], concentration [22], and focus [23] on a colloidal system.

Taking all the above into account, we present a microfluidic chip based on optical detection. During this work, we simulated the design and physical behaviour of the device in COMSOL Multiphysics software. Then, we use a combination of photolithography, and moulding on PDMS material to build the microfluidic system. This device has different coupled geometries that perform mixing, separation, concentration, focus and detection functions. Consequently, this microfluidic device can be used as a non-invasive screening method for the detection of cancer cells from the respiratory tract in saliva samples that, unlike other methods, this system applies microfluidic technology.The novelty of the microfluidic device developed in this work includes an arrangement of different geometries that work together managing particles of interest inside a fluid, that simulate non-small cancer cells and contrast it with computational modeling

2 Materials and Methods

Following our objective of developing a screening method for cancer cell detection, we have to define the operations required in the device. For this, we look into the different operational units within the microfluidic field. Some operational units are used to mix, separate, focus, react and concentrate. These designs can be categorized by active or passive methods to work. The active methods work by the influence of external forces influencing the fluid or its content, facilitating the operational process. The passive method depends only on the configuration of the geometrical design and the fluid parameters to operate on the input fluid.

For our objective, we propose that our requirements include the mixer, separator, concentrator, and finally the focusing operational units. We aim first to mix the saliva sample, which is diluted in serum, with the biomarker sample. Two passive methods that serve this purpose include the linear and the serpentine geometries. These can be accompanied with grooves for the correct mixing of substances in microchannels as used by many authors such as A. Kumar et al. [24]. In this kind of geometries, the developed laminar flow, the length of the microchannel, dimensions, and the diffusion coefficient, play a fundamental role in the appropriate mixing.

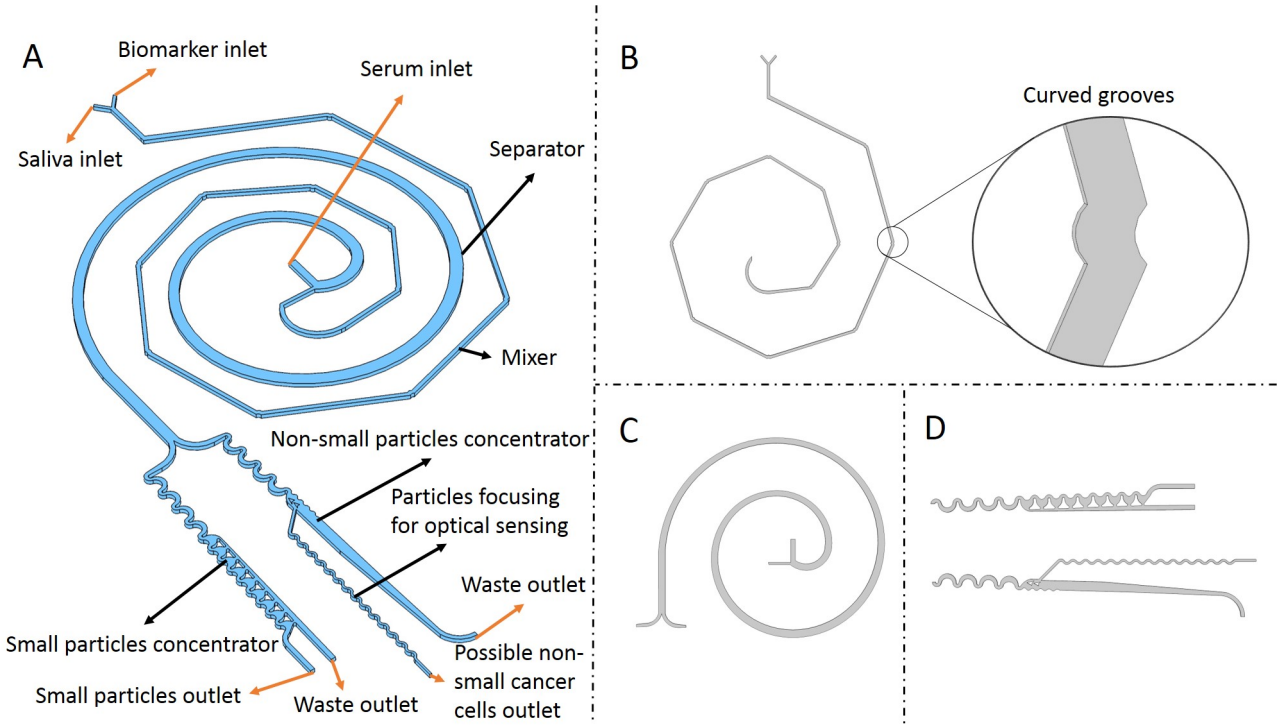

Figure 1: Chip design with coupled geometries: A) Concept design and description of its parts. B) Mixer, Spiral microfluidic geometry and curved grooves. C) Separator, spiral geometry. D) Top: pre-concentrator and concentrator for small particles. Bottom: pre-concentrator and concentrator for big particles, including the focus stream for non-small cancer cells.

After the mixer geometry, it is necessary to couple a separator for sorting components inside the channel to separate them.Particle separation by passive methods can be done by inertial migration, hydrodynamic filtration, cross-flow filtration, deterministic lateral migration, gravity or viscoelastic separation [25]. The spiral design is one of the inertial sorting geometries. Sorting particles or cells by migration are also called Dean Flow Fractional [26].

Spiral geometries contemplate a Dean flow in laminar fluids, where the velocity differences within the channel, as a result of the interaction between the Dean drag force and the lift force, create a velocity gradient where the particles with different mass are influenced and separated [27–29].

The next stage is the two concentration units. The first one will reduce the volume of the sample, increasing the concentration of the cancer cells, therefore, increasing the sensing sensitivity. One of the characteristics of this stage is that it must be a continuous process, considering that it would fit at the end of the separator. J. Martel et al. investigated the operation of geometry for passive systems that can concentrate polystyrene particles following a continuous concentration system and concentrated cells. In this way, they managed to reduce the volume by 75% [30].

Finally, the concentrated particles in the flow of cancer cells must be aligned to increase the probability of optical detection. This increased chance is the reason why serpentine geometries are used to align particles in two dimensions, and the existence of systems that manage to confine particles in a single beam. However, favourable results have been obtained in serpentine geometries for narrow channels without the influence of external forces [23]. This geometry exploits inertia for focusing particles. However, this geometry can also operate as a sorting unit if not appropriately designed. This behaviour occurs because the drag and lift force influence the fluid, and hence, the particles inside [21, 31]. Therefore, to avoid this effect, it is essential to design and simulate the microchannel [32].

Microfluidic systems are built based on extensively studied preestablished geometries. To approach a new field of study, we are in demand for alternative designs of TAS devices. For this reason, to create a system that can be applied in the medical field for the detection of cancer cells in saliva samples, it has been decided to reinvent the geometries to

achieve a compact device.

2.1 Computational modeling

We designed the microfluidic system and ran the simulations using the software COMSOL Multiphysics [33]. Our design (Fig.1A) aims to fulfil the different requirements of our device. The specific dimensions of the complete setup and microchannels can be seen in Table 1.

Dimensions (μm)				
Attrb.	Full chip	Mixer	Separator	Conct.
Length	1.75E+04	3.78E+04	3.37E+04	7.93E+03
Width	1.07E+04	1.00E+02	2.00E+02	varies
Height	1.00E+02	1.00E+02	1.00E+02	1.00E+02

Table 1: Chips designs dimensions

In the first step, we coupled a mixer and a separation unit. We propose and designed the mixer following a Fermat's spiral geometry, where half of the spiral consists of the mixing unit, and the other half is the standard spiral geometry as a separation unit. The advantage of this design is that the development of this structure requires one layer of PDMS material for the experimental step. This design includes the use of several segments connected using curved grooves. The design developed here can be seen in Fig.1B. To ensure that the mixing unit gives the expected output of the fluid, we verify the diffusion of the input fluids throughout the mixing unit by extracting concentration profiles through the microchannel and comparing the results against the experimental tests.
The second unit consists of the second half of the Fermat's spiral as represented in the Fig 1C; This is a standard spiral geometry that uses inertia in a fluid dominated by Dean drag force to separate particles by size. We use this size separation to highlight potential non-small cancer cells. The list of particle types that we use to simulate the colloidal fluid within the mixer includes non-small cancer cells ($16-20\ \mu m$), erythrocyte ($6-8\ \mu m$), and unattached biomarkers ($1\ \mu m$).
The third step consists of two operational concentrator units, as represented in Fig 1D. Each set handles different ranges of particle sizes. The first one receives as an input, particles smaller than $15\mu m$, while larger particles are guided into the second set. We focus our attention on the large particles, as these represent potential cancer cells, which are managed by the second set. The first set is designed following a traditional serpentine concentrator unit. The second set is a modified serpentine unit, designed to handle non-small particles. The modified unit benefits from the momentum carried by non-small particles. The output of this modification produces a concentrated stream which is then focused using a serpentine unit.

2.2 Experimentals procedure

Much of the methodology for making the chip in PDMS follows the procedure described by E. Pedrol [34]. The substrate was a silicon wafer (100 mm, Mitsubishi Silicon America), a positive photoresist AZ1505 (Merck, reactive grade), AZ726 MIF Developer, (Merck $> 25\%$ in H_2O and surfactants) and acetone (reactive grade) were used. A spin coater POLOS for the spin coating of the photoresist was handled. The equipment for making the mas was A maskless lithography equipment Heidelberg DWL66Fs with a diode laser of 405 nm with a power intensity of 20 mW. The laser is 3 % the original power intensity after a filter prior to reaching the holder sample.
The microchannels were made with 3 inches silicon wafer where they were dehydrated for 1 hour in a hot plate at 100° Celsius (100 mm, Mitsubishi Silicon America), then a spin coating for the structure fabrication was used in order to prepare the resin to make the UV exposure.The first layer applied was a OMNICOAT (Omni-Coat, MicroChem Corp.). OMINOCAT acts as an adhesion-promoting agent. Subsequently, The silicon wafer was coated with the SU8 resin (SU8 2150, MicroChem Corp). The patterns were transferred from the mask to the SU8 resin through UV exposure. The UV exposure was performed with a mercury discharge lamp (MG 1410, Karl Suss). The silicon wafer was then developed in PGMEA solvent (AZ® EBR Solvent) to remove the resin in excess. A reactive ion etching (RIE) (PlasmaPro NGP80, Oxford Instruments) was used to remove and clean the wafers, leaving only the patterns over the silicon wafer.
The SU8 master was deposited at the bottom of an aluminium container to be coated by PDMS (Sylgard 184, Dow Corning). Previously, a 20 ml mixture of PDMS resin with 2% by weight of catalyst for each SU8 master was degassed for one hour. The mixture was then poured into the aluminium container, completely covering the SU8 master, leaving it to cure for 2 hours at 80° Celsius to speed up the polymerization process. The PDMS layer was subsequently removed. Each ge-

ometry was established as an independent chip; therefore the surface of the four PDMS chips were exposed to RIE generated oxygen plasma to bond the roof layer with the patter layer under the following conditions: Power: 20 W, oxygen flow rate: 35 sccm, pressure: 50 mTorr and time: 30 s.

3 Results and discussion

The results of the two sections studied are presented below. First, we show the computational part, followed by the experimental procedure and results in the second part. Through this research, we highlight the importance of preliminary computational modelling of the experimental procedure as the means to save resources in building microfluidic devices.

3.1 Computational procedure

The first designed geometry consists of a linear system with grooves, where each groove introduces a tilt to the linear system of next sequence forming the first half of the Fermat spiral. This first half works as a mixer, as shown in Fig.2.

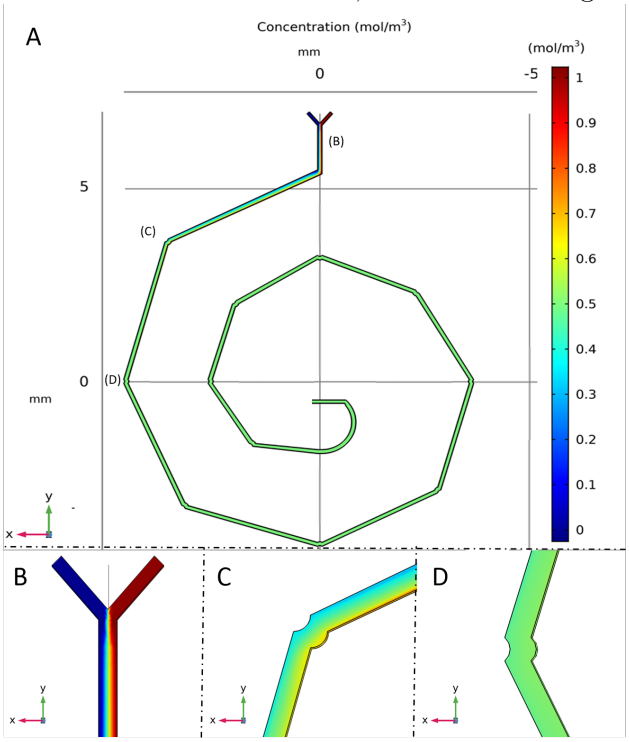

Figure 2: Concentration profile for the mixer unit (mol/m^3). A)Complete mixer concentration profile. B) Inlet concentration profile. C) First groove, concentration profile. D) Second groove, concentration profile.

Using COMSOL Multiphysics software, Navier Stokes' equations for designed 3D geometry have been numerically approximated. In this case, a fluid inlet pressure of 126 mbar was used. After obtaining the velocity profile, the software was able to calculate the diffusion profile using the convection-diffusion equation (C-D) Eq(1).

$$\frac{\partial C}{\partial t} = D\nabla^2 C - \nabla(\vec{u}C) \tag{1}$$

Where C refers to the concentration of the solute, D is the diffusion coefficient and vector u is the velocity profile. This system is comprised of a typical Y-junction inlet. However, the grooves that deflect the channel creating a spiral are not a conventional design proposed in research on mixers within the microfluidic community. According to the simulation, the grooves, the length, and the narrow channel are factors required for proper mixing [35]. Although the two fluids mix progressively along the channel, when a transverse section is made to the trajectory of the fluid as shown in Fig.3, the fluid mixture presents a different concentration behaviour from that described in Fig.3.

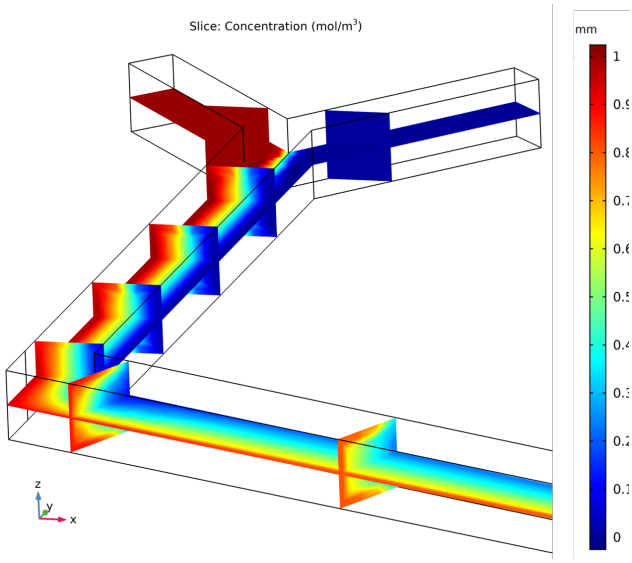

Figure 3: Transverse concentration profile to the fluid trajectory for the mixer unit.

This change in the angle of the fluid trajectory causes a lateral instability that leads to a transversal flow field (Dean flow). This instability occurs due to the balance between viscosity and inertial forces, generating vortices within the channel [36, 37]. This phenomenon also occurs in each groove, which improves the mixing process. However, after each groove, this profile returns to behave as in Fig.2.
The next geometry studied corresponds to the second half of the Fermat spiral.

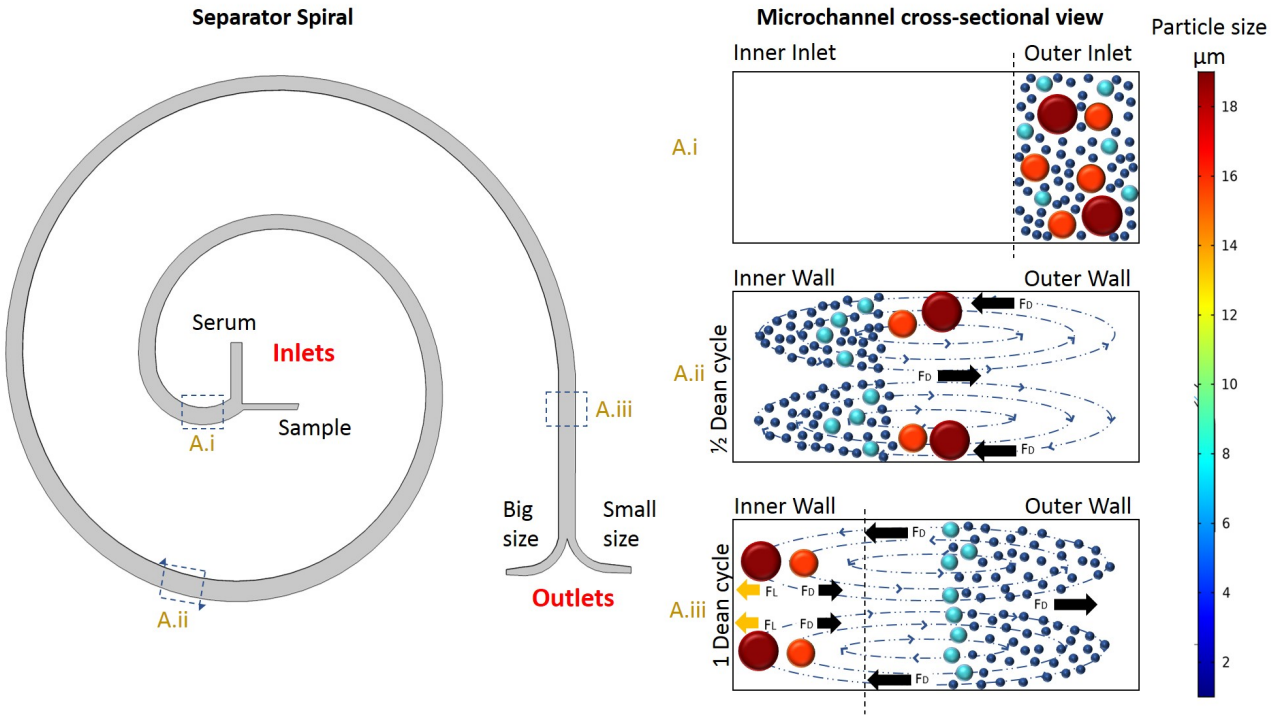

Figure 4: Schematic illustration of the separation principle for high throughput big sizes particles sorting using (DFF) Dean Flow Fractionation. The marked sample and the high-pressure diluting fluid (serum) enter the centre of the spiral. A.i) in the initial part of the separator, the particles are confined to the outer wall. A.ii) Under the influence of Dean drag forces, particles migrate along the Dean vortices to the inner wall. A.iii) large particles are confined to the inner wall where they experience additional strong inertial lift forces (FL) and Dean drag forces (FD). In contrast, smaller particles are influenced to a lesser extent by inertial forces.

The function of this design is to classify the particles by size, taking into account particle density and size. In this category of spiral designs, the Dean flow plays a fundamental role because a vortex created inside the channel throughout the design makes possible the particles sorting [37].

Considering the final function of the device, biomarkers unattached to cancer cells are required to be discarded to evade false-positives in the optical sensing, as well as the non-cancer cells. Therefore, we consider small particles, such as these unattached biomarkers, and the large particles of interest.

The range of sizes led to employ the particles tracing for fluid flow module of COMSOL Multiphysics to establish the drag forces and lift forces for our particles simulation. Four particle types were determined according to size: 2 μm particles resembling the biomarker; 6 μm particles simulating non-cancerous epithelial cells, and particles of 15 μm and 20 μm representing non-small cancer cells.

The simulated particles underwent different pressures to vary the velocity and to have an adequate Dean flow, leading to a proper separation by size. Fig.4 reflects how the particles are classified in a curved channel using Dean flow fractionation DFF.

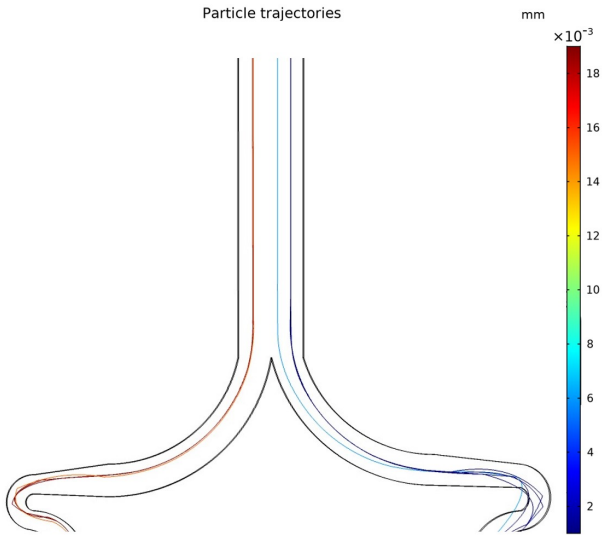

Figure 5: Separator ending. Left stream for the particles above 15 μm, right stream for particles below 15 μm.

The simulation results showed an adequate separation process under a range of conditions for laminar fluids.After several simuations, the optimal values to carry out an ideal separation were de-

fined. it was established an inlet pressures higher than 252 mbar for the fluid containing the sample to be separated, and inlet pressures greater than 300 mbar for the diluent fluid. Keep in mind that confinement at the inlet of the separator is only achieved for an inlet pressure ratio of 1.2:1, below or above this ratio, the confinement in the outer wall of the separator will not be carried out.
Fig.5, represents the separation with a separator inlet pressure of 350 mbar for the diluent fluid, and 294 mbar for the colloidal sample. This set of conditions allowed the classification of the 15 and 20 μm particles against the inner wall, while particles of less size followed the outer wall.
The separation process can be described in terms of Dean cycles (DC). In each cycle completion, the particles return to their position in the cross-sectional plane within the channel. Only small particles complete a DC, as the non-small particles reach a point (half a DC) where the lift forces are dominant [26]. The nature of the sets of particles remains constant throughout the channel. The particles of interest are then separated from the rest.

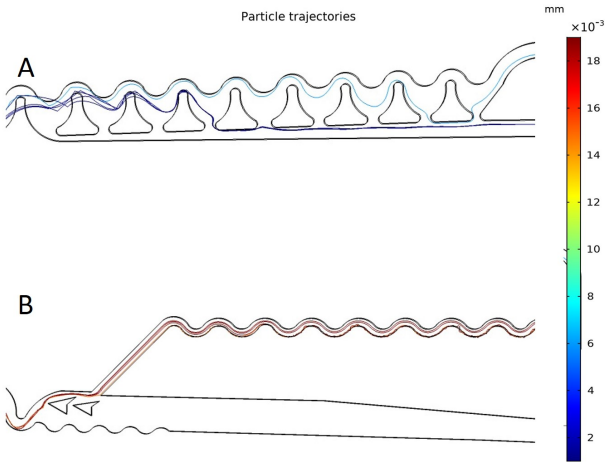

Figure 6: Particle trajectories in concentrator designs. The color scale indicates the particle size. the light blue line represents 2 μm particles, the dark blue line, 6 μm particles and, the red and dark red are 15 μm and 20 μm respectively. A) Small particle concentrator with siphons to remove liquid. B) Large particle concentrator with an expansion to guide particles by momentum and reduce the liquid.

The next computational process was carried out in the concentrating unit. For this section, a small particle concentrator (Fig.6A) has been created to balance the pressure within the system and avoid the influence of the particles by pressure drop. For our interest, the small particle concentrator exists only to balance pressure at the separator outlet with no further use. However, we could focus small particles instead, as this functionality depends on the input pressure of the mixer, leaving open the possibility of recovering the biomarker. The continuous flow microparticles concentrator for small particles was designed followed the study conducted by J. Martel and K. Smith [30]. The focusing unit based on inertial volume reduction has a series of siphons to remove the fluid in the particles free region of the focusing units.

The functionality of the concentrator units is a tradeoff between both small and large particle concentrator, as a consequence of being coupled to the separator. The optimum flow for each set requires contrasting initial conditions. A non-optimum selection of the conditions in a unit leads to different particle trajectories. An example of this situation is seen in Fig.6, where an optimum selection of conditions for the large particle concentrator (Fig.6B) influences the trajectories in the small particle concentrator (Fig.6A). This example is the consequence of high flow pressure in contrast to the optimal values required of the small particle concentrator [30]. One way to solve this problem might reside on the length of the outer wires in the outlet section, which reduces or increase the pressure drop in that section. However, this could potentially destabilize the entire system.

In our work, we focus our attention into the functionality of the large particles concentrator. The concentrator works properly for pressures above 300 mbar. Inertial forces in the expansion section move larger particles towards the non-small cancer cell outlet [26, 27], causing the particles to go into the output stream to be confined as can be seen in Fig.6B. Prior to the concentrator expansion that sorts the particles, the geometry starts with a serpentine segment that aligns particles. Close to the upper wall arise a bifurcation. The narrowest section is where the particles focusing unit begins, see Fig.6B and it can be seen in detail in Fig.7. This unit confines large particles in a single line. This is a product between the migration of particles along with the Dean vortex, and the switching of the vortex direction caused by serpentine curvature in the opposite direction [26, 31]. The numerical model made in COMSOL multiphysics manages to confine the particles along the focuser. A comparison between the three sections of the serpentine geometry allows further analysis of the confinement effect. In Fig.7A1, particles coming from the concentrator decreasing their speed due to the

high pressure drop in this geometry.However, particles are not aligned when entering this confiner. Then, in section Fig.7A2, particles begin to be influenced by Dean vortices, aligning themselves in areas within the canal. Finally, in the last part (Fig.7A3) particles are found aligned in a single beam. It is essential to recognize that this confinement is carried out only in two dimensions; as a consequence, particles can move freely along the Z-axis (micro-channel height).

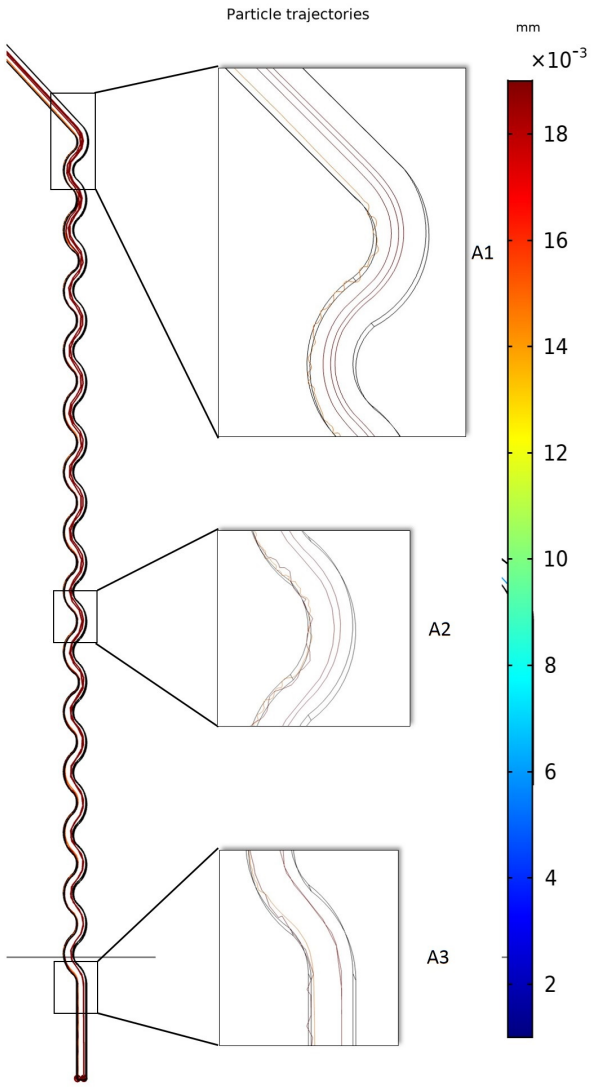

Figure 7: Large particle trajectories for the concentrated stream in the focusing section. A1) Inlet coupled to the concentrator without aligned particles. A2) Particles migrating and organizing due to Dean vortex. A3) fully aligned particles.

The use of a narrow channel constrains the size of the Dean vortices to resemble the size of the large particles. This is a fundamental factor towards increasing the probability of locating particles in the centre of the channel, i.e. the two vortices are the closest, and the cross-sectional velocity field is maximum.

3.2 Mask, Mold and PDMS designs

The nano-fabrication equipment and methods allowed to create the mask with four designs [Complementary Material] corresponding to the mixer, separator, concentrators, and the full chip. This mask was used to make the master mould. The thickness of each geometry was measured using confocal laser scanning microscopy (CLSM) where the mixer, separator, concentrator and full chip yielded the following results 104 μm, 102 μm, 108 μm, 98 μm respectively. The designs used were the same as those presented in S3. Once the elaboration of the device is completed, we are enabled to carry out the experimental tests and compare them with the theoretical models.

3.3 PDMS Mixer unit operation

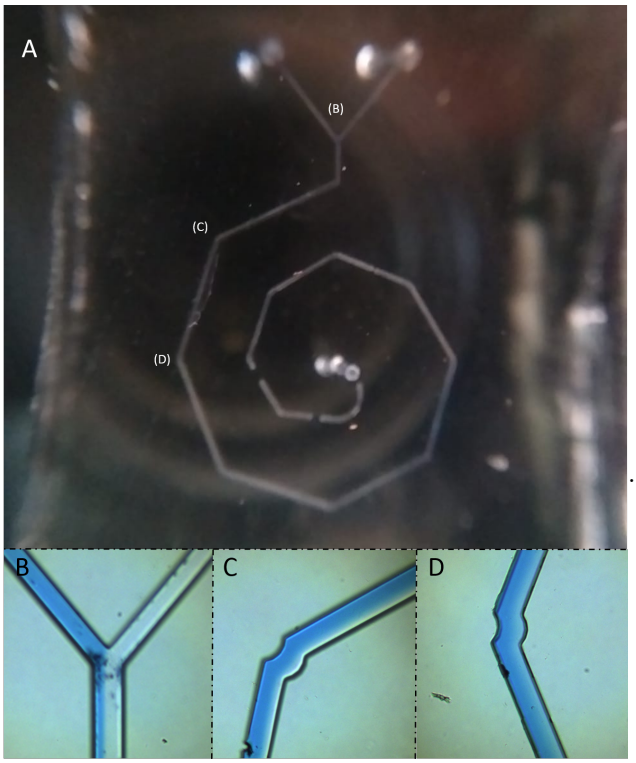

Figure 8: Experimental behaviour inside the microchannel of the mixer between two fluids, water and dyed water. A) Complete mixer microchannel. B) Inlet diffusion profile. C) First groove, diffusion profile. D) Second groove, diffusion profile

The mixer is one of the main units of the set system with the separator. Given that there are inlets current flow in both, it is essential to know if they behave adequately in a wide pressure range.

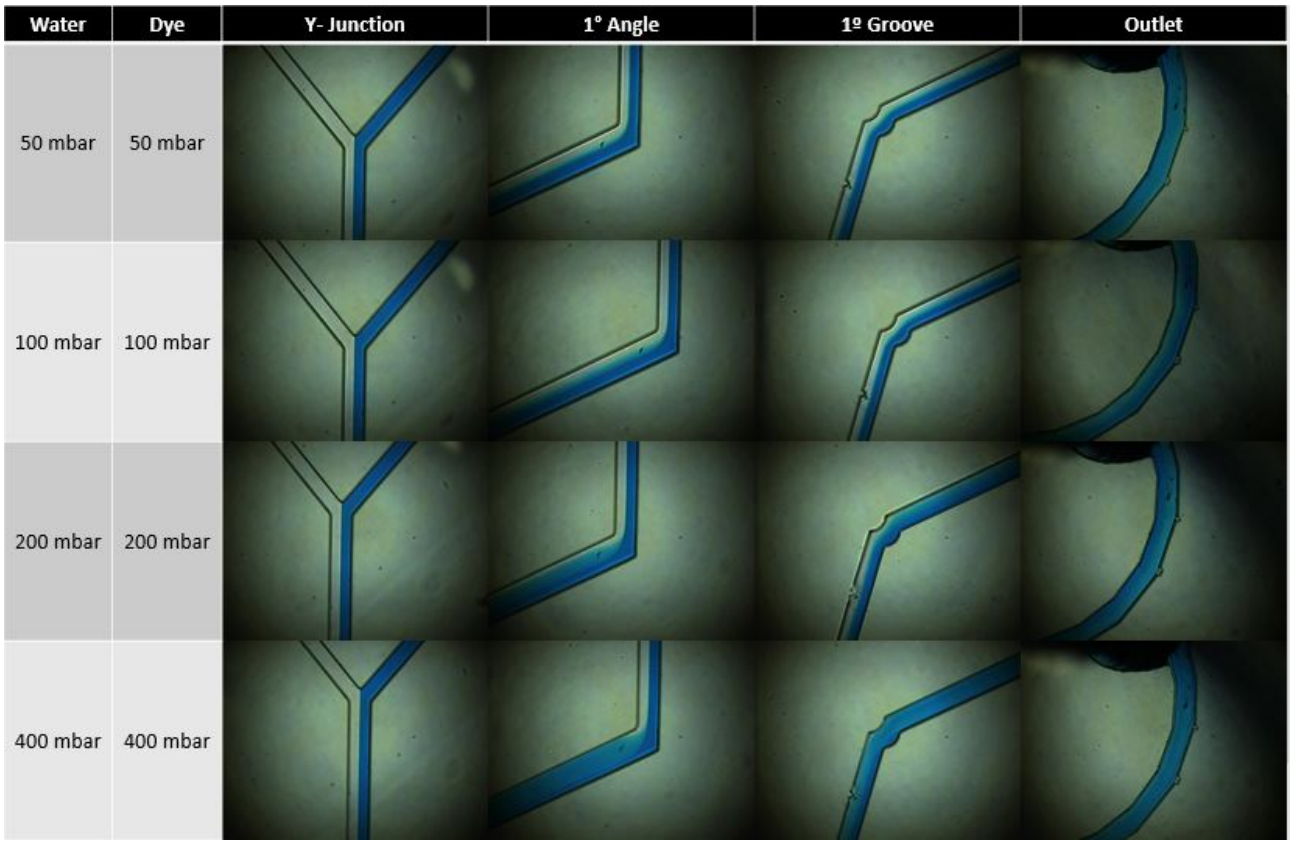

Figure 9: Experimental study of the mixer varying the inlet pressure. The left column represents the inlet pressures in millibar. The measurement points are at the Y-junction inlet, the first angle, the first groove, and the mixer output. As pressure is increased, the fluid mixes earlier within the unit.

As the mixer is made up of two inputs, the inlet pressure of both must be considered as acting as one unit. The reason why the mixer must have a wide operating range is that the outlet pressure of the fluid in this geometry must be manipulated depending on the conditions of the serum inlet to have an intended separation process. For this, if the fluid fails to mix properly throughout the mixer, then biomarker particles will not couple to the cancer cells, causing the sensing to be null.

One of the advantages of Fermat's spiral in the numerical model is that, regardless of the input velocity or input pressure, the length, grooves and the narrowness of the channel, allows the two inlet fluids to mix successfully when entering to the separator, this can be observed in the pressure study (S1).

In this numerical model, the mixing process reaches a homogeneous concentration profile in earlier stages of the unit as the inlet pressure increases. The study consisted of varying the pressure of inlets flows from 100 mbar to 800 mbar. It was observed considerable improvement in mixing time. These results were compared with an experimental study of the same nature verifying the results, as seen in Fig.9.

Once the pressure study is completed, we study the role of input flows in specific inlets by interchanging the input flows and checking the output performance.Contrasting Fig.9 and Fig.8, It can be seen that regardless of the order of fluid entry, the fluid will mix thoroughly. These same results can be contrasted with Fig.2B, Fig.2C and Fig.2D. In this way, we demonstrate that the grooves in a narrow channel are appropriate for proper mixing since they speed up the mixing process [24]. Likewise, the angle at the beginning benefits the mixing process because it generates Dean vortexes. Also, as the fluid progresses, these vortexes will be generated in each groove in agreement with the numerical study.

3.4 PDMS Separator unit operation

The separator has been studied through two tests: A ratio study, and a pressure study for optimal separation. The first consisted of studying the relationship of the inlet flows as can be seen in Fig.10, to obtain the relative conditions that best

confines the sample fluid in the external wall at the inlet of the separator. Aiming for the functionality of the mixer in a wide range of pressures for the second study, we varied the inflows pressure maintaining the ratio between inputs. Fig.11, shows the results obtained with the best inlet pressures.

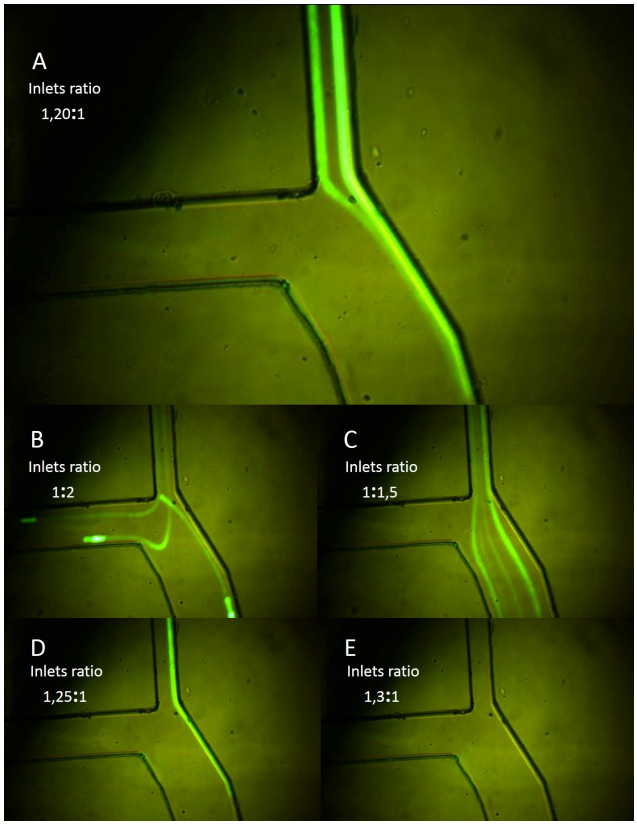

Figure 10: Inlets ratio study between fluid containing the sample and the diluent fluid to confine the sample to the outer wall in the beginning of the separator. A) 1.20:1, B) 1:2, C) 1:1.5, D) 1.25:1, and E) 1.3:1 water to sample experiments.

Fig.10, shows the result of the first study. The functional situation is shown in Fig.10A, which uses a 1.2:1 ratio W/S (Water/Sample), where the sample stream is confined to the outer wall of the inlet. This confinement is necessary for an optimal separation [26]. This behaviour is observed in the numeric model and is explained in detail in Fig.4. One of the cases studied was the behaviour of the profile when the sample inlet pressure was much higher than the water inlet pressure. In Fig.10B, a ratio of 1:2 can be seen. This configuration causes the sample stream to be directed toward the inlet of the water, preventing it from entering and changing the direction of the inlet flow of the water. When the ratio is 1:1.5 (Fig.10C), the water flow is confined to the inner wall, which does not give an adequate separation process. Alternatively, the water entering the sample inlet occurs when the water flow is much higher. This is the case of a water ratio 1.3 times higher than the sample pressure (Fig.10E). However, by reducing this ratio to 1.2:1, the particle flow is confined, water is also backset to sample stream as seen in Fig.10D. The detailed results of the second study can be seen in Table 1 of the supplementary material. The study consisted of 14 tests. Seven tests are used with samples containing $5\mu m$ particles, and the other seven experiments with $20\mu m$ particles. In both cases, the inlet pressure of the diluent fluid (water) was varied from 50 to 350 mbar. Likewise, the sample inlet pressure ranged from 42 mbar to 294 mbar. In all cases, the optimal ratio of 1.2:1 was maintained. The same behaviour was observed compared with the numerical model. In this way, the separation becomes optimal as long as the sample inlet pressure is above 252 mbar.

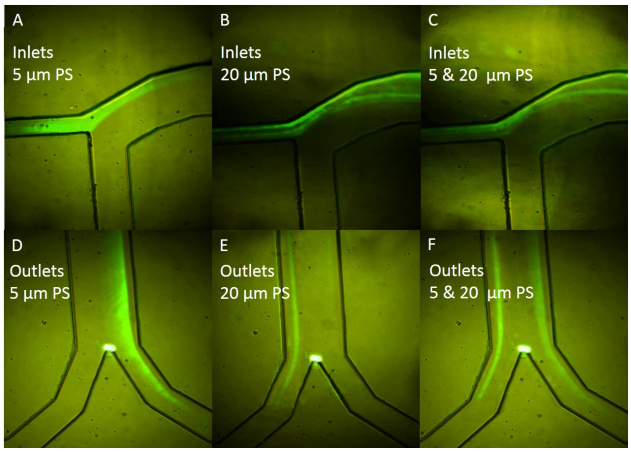

Figure 11: Particles behaviour in the separator for inlet pressures of 350 mbar (diluent fluid), and 294 mbar (sample). A) Inlets for the confined particle profile of $5\mu m$. B) Inlets for particle profile of $20\mu m$. C) Inlets for the mixture of particles between 5 and $20\mu m$. D) Outlets with $5\mu m$ particles. E) Outlets with $20\mu m$ particles. F) Outlets with a mixture of particles between 5 and $20\mu m$ where the largest particles are correctly separated towards the left exit

According to the results of the pressure study, the pressure values which the separation profile was optimum (350mbar and 294 mbar) were used, and the 1.2:1 W/S ratio is also maintained. As a result, the sample stream was confined to the outer wall of the separator inlet, and the particles were separated at the outlet. Figures 11A and 11D, show the results obtained with the mentioned conditions when $5\mu m$ particles are introduced. The small particles are separated towards the outer wall of the spiral after completing a Dean cycle. Similarly, figures 11B and 11E, are the result of introducing $20\mu m$ particles into the system. Likewise, separa-

tion takes place for these large particles. However, the larger particles are separated towards the inner wall of the spiral after completing a Dean cycle. Finally, Figures 11C and 11F, are one of the most representative images of the separator, since this time a mixture consisting of 0.11% PS of $5\mu m$, 0.11% PS of $20\mu m$ and 99.77% water is introduced as a sample. The latter experiment results in the proper sorting of the particles by size. The inner wall current (left) at the outlet of the separator corresponds to the $20\mu m$ particles while the current on the right corresponds to the $5\mu m$ particles. This data corroborates the results of the numerical simulation.

3.5 PDMS Concentrator and focusing Unit

The large particles that make up the left stream at the end of the separator is composed of particles from 15 to $20\mu m$, which represent sizes of non-small cancer cells [26, 38]. In this experiment, we use 0.11% of particles in aqueous solution. In reality, saliva samples contain slightly less concentration of particles than in our experiment. Hence it is necessary to concentrate the particles to increase the sensitivity. This is achieved thanks to a geometry that works as a concentrator, which considerably removes the diluent fluid. The concentrator is composed of a serpentine section designed after the concentrator in the numeric model.

As can be seen in Fig.12A, particles behave in the same way as the simulation in COMSOL Multiphysics (Fig.6B). However, it is also possible to appreciate additional particles behaviour, where they deviate from the trajectory and choose to follow an interruption in the channel (Fig.12B). In these exceptions, the particle trajectory later adopts the expected path, and the particles are concentrated. This new behaviour must be related to the pressure of the fluid, as mentioned by authors such as J. Martel and K. Smith [30]. The concentrator requires an optimal pressure to make correct confinement of particles.

Finally, the focusing unit is coupled to the concentrator. Particles ejected towards the left wall of the concentrator, enter a long serpentine where they are confined. Fig.12 shows how the particles are aligned at the end of the section. However, when observing the velocity within the confiner, it was apparently higher than expected. Despite the results, it would be ideal to run more tests on this system to corroborate the results. It should be considered that the operation of the confinement unit should be carried out in conjunction with the concentrator. It is essential that both work correctly with the input conditions of the concentrator.

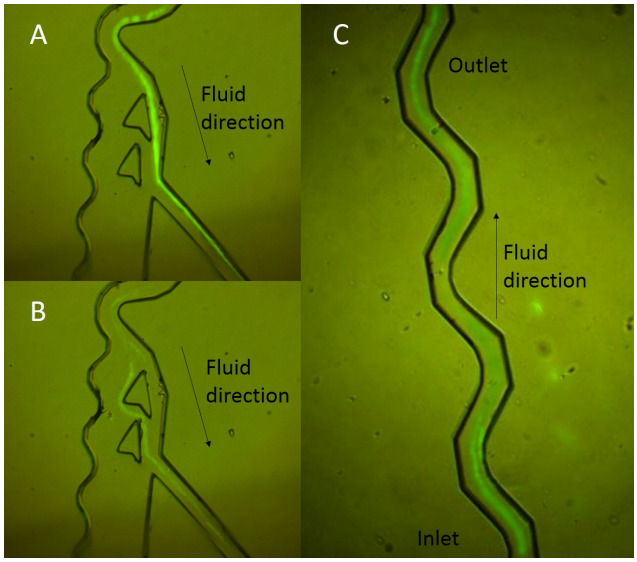

Figure 12: Fluorescent detection of PS particles in concentrating and focusing unit. A) normal behavior with large particles. B) Deviation in particles trajectory. C) Focusing unit with PS particles.

4 Conclusions

We present a study on the microfluidic units that potentially can be combined into a TAS device for respiratory tract cancer screening using saliva samples. First, we define the functionalities are required from each unit required for cancer screening procedure. We design the geometries of the operational units of interest: mixer, separator, and a concentrator coupled to a focuser unit. Then, we perform a fluid dynamics numerical modelling of each unit using COMSOL Multiphysics to check for optimal design and functionality of the units under the conditions set to work for the colloidal system of interest. We test the units by performing a pressure study on the separator and the mixer. Afterwards, we build the TAS units separately and we verify the numerical results against experimental observations. We perform additional tests on the physical separator unit to characterize the particle response to initial conditions. The particles of interest have sizes of 15 μm and 20 μm, we simulated and experimentally tested the behaviour of particles of 5 μm and 20 μm independently and in a combined manner to check for correct mixing, and proper separation.

Our proposed mixer unit design, based on a combination of linear channels linked with grooves that follows a half Fermat spiral, do not require an increase on the channel length when the pressure applied to the flow is increased, in contrast to traditional mixer units designs. The narrowness of the channel and the use of grooves are the main factors of proper mixing due to their effects on the Dean flow, which allows a wide functionality spectrum.

The separator follows a traditional spiral design, complemented with the mixer to form a full Fermat spiral. The advantages of the coupled system mixer-separator following this design leads to a compact microfluidic device. This arrange requires less materials than other solutions, and leads to fast device response due to the fact that the device works in a high pressure range for the compact scales we work on.

We make use of a set of a small particle concentrator unit, and a non-small particle concentrator-focuser unit. We proposed a novel design of the non-small particle concentrator of continuous fluid flow, that also integrates a focuser unit design. Both units are entangled by a tradeoff between the concentrator functionality and the inlet conditions of the set.

Recent advances of particle modelling simulations within fluids drastically contributes towards realistic modelling of colloidal systems in microdevices, more specifically the inclusion of lift forces in fluid dynamic simulations. Thanks to both studies, we are able to perform cost-efficient research of TAS devices.

5 Future directions

For future work, the ideal is to test the concentrator with different pressure parameters, to optimize the device separation. Furthermore, it is essential that the surface of the micro-channels is not rough so that the particles do not stick along the channel. On the other hand, to develop a device that might function as a detection method, it is essential to couple the optical fibers to emit and detect light signals. In addition, make the circuit so that this device is independent and compact. Finally, once all the parameters are appropriate, clinical studies should be conducted to verify the usefulness, scope, and limitations of the device.

6 Acknowledgements

I greatly appreciate the contributions of Jorge Nicolas Hayek Valencia and Eric Pedrol.

References

[1] M. Pizzanelli, "Overscreening or prevention in a human scale? Excessive screening," *Revista Brasileira de Medicina de Família e Comunidade*, vol. 10, no. 35, pp. 1–7, 2015.

[2] J. M. G. Wilson, G. Jungner, and W. H. Organization, *Principles and practice of screening for disease*. Public health papers ; no. 34, World Health Organization, 1968.

[3] D. J Hunter, *Epidemiology of Cancer*, vol. 27. Elsevier Inc., twenty-six ed., 2008.

[4] T. B. Richards, A. Soman, C. C. Thomas, B. VanFrank, S. J. Henley, M. S. Gallaway, and L. C. Richardson, "Screening for Lung Cancer 10 States," *MMWR. Morbidity and mortality weekly report*, vol. 69, no. 8, pp. 201–206, 2017.

[5] F. Bray, J. Ferlay, I. Soerjomataram, R. L. Siegel, L. A. Torre, and A. Jemal, "Global cancer statistics 2018: Globocan estimates of incidence and mortality worldwide for 36 cancers in 185 countries," *CA: A Cancer Journal for Clinicians*, vol. 68, no. 6, pp. 394–424, 2018.

[6] D. Ettinger, "Lung Cancer and Other Pulmonary Neoplasms," *Goldman's Cecil Medicine: Twenty Fourth Edition*, vol. 1, pp. 1264–1272, 2011.

[7] E. F. Patz, P. Goodman, and G. Bepler, "Screening for Lung Cancer," *Massachusetts Medical Society*, vol. 343, no. 22, pp. 1627–1633, 2003.

[8] R. D. Kellerman, D. Rakel, and E. A. Gillaspie, *Lung Cancer Method*. No. November, Elsevier, 2020.

[9] A. Ruano-Ravina, M. Pérez-Ríos, P. Casàn-Clará, and M. Provencio-Pulla, "Low-dose CT for lung cancer screening," *The Lancet Oncology*, vol. 19, no. 3, pp. 131–132, 2018.

[10] K. Qian, Y. Wang, L. Hua, A. Chen, and Y. Zhang, "New method of lung cancer detection by saliva test using surface-enhanced Raman spectroscopy," *Thoracic cancer*, vol. 9, pp. 1556–1561, nov 2018.

[11] E. Vargas-Obieta, J. C. Martínez-Espinosa, B. E. Martínez-Zerega, L. F. Jave-Suárez, A. Aguilar-Lemarroy, and J. L. González-Solís, "Breast cancer detection based on serum sample surface enhanced Raman spectroscopy," *Lasers in Medical Science*, vol. 31, no. 7, pp. 1317–1324, 2016.

[12] F. Wei, C. C. Lin, A. Joon, Z. Feng, G. Troche, M. E. Lira, D. Chia, M. Mao, C. L. Ho, W. C. Su, and D. T. W. Wong, "Noninvasive saliva-based EGFR gene mutation detection in patients with lung cancer," *American Journal of Respiratory and Critical Care Medicine*, vol. 190, no. 10, pp. 1117–1126, 2014.

[13] H. A. Soini, I. Klouckova, D. Wiesler, E. Oberzaucher, K. Grammer, S. J. Dixon, Y. Xu, R. G. Brereton, D. J. Penn, and M. V. Novotny, "Analysis of Volatile Organic Compounds in Human Saliva by a Static Sorptive Extraction Method and Gas Chromatography-Mass Spectrometry," *Journal of Chemical Ecology*, vol. 36, no. 9, pp. 1035–1042, 2010.

[14] T. Bayraktar and S. B. Pidugu, "Characterization of liquid flows in microfluidic systems," *International Journal of Heat and Mass Transfer*, vol. 49, no. 5, pp. 815 – 824, 2006.

[15] G. Lujia, F. Jinsong, F. Zecong, X. Jie, and L. Xiaonan, "Application of microfluidic "lab-on-a-chip" for the detection of mycotoxins in foods," *Trends in Food Science Technology*, vol. 46, no. 2, Part A, pp. 252 – 263, 2015.

[16] P. S. Dittrich, K. Tachikawa, and A. Manz, "Micro total analysis systems. latest advancements and trends," *Analytical Chemistry*, vol. 78, no. 12, pp. 3887–3908, 2006. PMID: 16771530.

[17] J. Connelly, S. Kondapalli, and M. Skoupi, "Micro-total analysis system for virus detection: microfluidic pre-concentration coupled to liposome-based detectionr," *Anal Bioanal Chem*, vol. 402, no. 402, p. 315–323, 2012.

[18] E. Eriksson, J. Enger, B. Nordlander, N. Erjavec, K. Ramser, M. Goksör, S. Hohmann, T. Nyström, and D. Hanstorp, "A microfluidic system in combination with optical tweezers for analyzing rapid and reversible cytological alterations in single cells upon environmental changes," *Lab Chip*, vol. 7, pp. 71–76, 2007.

[19] P. Thurgood, J. Y. Zhu, N. Nguyen, S. Nahavandi, A. R. Jex, E. Pirogova, S. Baratchi, and K. Khoshmanesh, "A self-sufficient pressure pump using latex balloons for microfluidic applications," *Lab Chip*, vol. 18, pp. 2730–2740, 2018.

[20] B. Finlayson, A. Aditya, V. Brasher, L. Dahl, H. Dinh, A. Field, J. Flynn, C. Jenssen, D. Kress, F. Ninh, A. Nordmeier, H. Song, and C. Yuen, "Mixing of Liquids in Microfluidic Devices," in *Proceedings of the COMSOL Conference 2008 Boston Mixing*, pp. 1–18, 2008.

[21] J. Zhang, S. Yan, R. Sluyter, W. Li, G. Alici, and N.-T. Nguyen, "Inertial particle separation by differential equilibrium positions in a symmetrical serpentine micro-channel," *Scientific Reports*, vol. 4, no. 1, p. 4527, 2014.

[22] B. K. Lin, S. M. McFaul, C. Jin, P. C. Black, and H. Ma, "Highly selective biomechanical separation of cancer cells from leukocytes using microfluidic ratchets and hydrodynamic concentrator," *Biomicrofluidics*, vol. 7, no. 3, pp. 17–20, 2013.

[23] J. Zhang, W. Li, M. Li, G. Alici, and N.-T. Nguyen, "Particle inertial focusing and its mechanism in a serpentine microchannel," *Microfluidics and Nanofluidics*, vol. 17, no. 2, pp. 305–316, 2014.

[24] A. Kumar, G. Prakash, R. Mandal, and V. Ranjan, "Effect of Geometry of the Grooves on the Mixing of Fluids in Micro Mixer Channel," in *COMSOL Conference*, pp. 1–7, 2012.

[25] J. Zhou, P. Mukherjee, H. Gao, Q. Luan, and I. Papautsky, "Label-free microfluidic sorting of microparticles," *APL Bioengineering*, vol. 3, no. 4, p. 41504, 2019.

[26] H. W. Hou, M. E. Warkiani, B. L. Khoo, Z. R. Li, R. A. Soo, D. S. W. Tan, W. T. Lim, J. Han, A. A. S. Bhagat, and C. T. Lim,

"Isolation and retrieval of circulating tumor cells using centrifugal forces," *Scientific Reports*, vol. 3, pp. 1–8, 2013.

[27] D. Di Carlo, "Inertial microfluidics," *Lab Chip*, vol. 9, no. 21, pp. 3038–3046, 2009.

[28] A. Mihandoust, N. Maleki-Jirsaraei, S. Rouhani, S. Safi, and M. Alizadeh, "Improvement of size-based particle separation throughput in slanted spiral microchannel by modifying outlet geometry," *Electrophoresis*, vol. 41, no. 5-6, pp. 353–359, 2020.

[29] N. Xiang, J. Wang, Q. Li, Y. Han, D. Huang, and Z. Ni, "Precise Size-Based Cell Separation via the Coupling of Inertial Microfluidics and Deterministic Lateral Displacement," *Analytical Chemistry*, vol. 91, no. 15, pp. 10328–10334, 2019.

[30] J. M. Martel, K. C. Smith, M. Dlamini, K. Pletcher, J. Yang, M. Karabacak, D. A. Haber, R. Kapur, and M. Toner, "Continuous Flow Microfluidic Bioparticle Concentrator," *Scientific Reports*, vol. 5, no. 1, p. 11300, 2015.

[31] D. Yuan, R. Sluyter, Q. Zhao, S. Tang, S. Yan, G. Yun, M. Li, J. Zhang, and W. Li, "Dean-flow-coupled elasto-inertial particle and cell focusing in symmetric serpentine microchannels," *Microfluidics and Nanofluidics*, vol. 23, no. 3, p. 41, 2019.

[32] J. Zhu, T.-R. J. Tzeng, G. Hu, and X. Xuan, "DC dielectrophoretic focusing of particles in a serpentine microchannel," *Microfluidics and Nanofluidics*, vol. 7, no. 6, p. 751, 2009.

[33] COMSOL INC S.A, *COMSOL Multiphysics®*. Stockholm, Sweden.

[34] E. Pedrol, G. Manuel, J. Massons, M. Nazarenus, L. Guerrini, J. Martínez, A. Rodenas, M. Aguiló, and E. al., "Optofluidic device for the quantification of circulating tumor cells in breast cancer," *Scientific Reports*, vol. 7, no. 7, p. 3677, 2017.

[35] J. Fan, S. Li, Z. Wu, and Z. Chen, "Chapter 3 - diffusion and mixing in microfluidic devices," in *Microfluidics for Pharmaceutical Applications* (H. A. Santos, D. Liu, and H. Zhang, eds.), Micro and Nano Technologies, pp. 79 – 100, William Andrew Publishing, 2019.

[36] V. Duryodhan, R. Chatterjee, S. Govind Singh, and A. Agrawal, "Mixing in planar spiral microchannel," *Experimental Thermal and Fluid Science*, vol. 89, pp. 119 – 127, 2017.

[37] N. Nivedita, P. Ligrani, and I. Papautsky, "Dean flow dynamics in low-aspect ratio spiral microchannels," *Scientific Reports*, vol. 7, no. 12, p. 44072, 2017.

[38] S. Zheng, H. Lin, J.-Q. Liu, M. Balic, R. Datar, R. J. Cote, and Y.-C. Tai, "Membrane microfilter device for selective capture, electrolysis and genomic analysis of human circulating tumor cells," *Journal of Chromatography A*, vol. 1162, no. 2, pp. 154 – 161, 2007. 21st International Symposium on Microscale Bioseparations.

Supplementary material

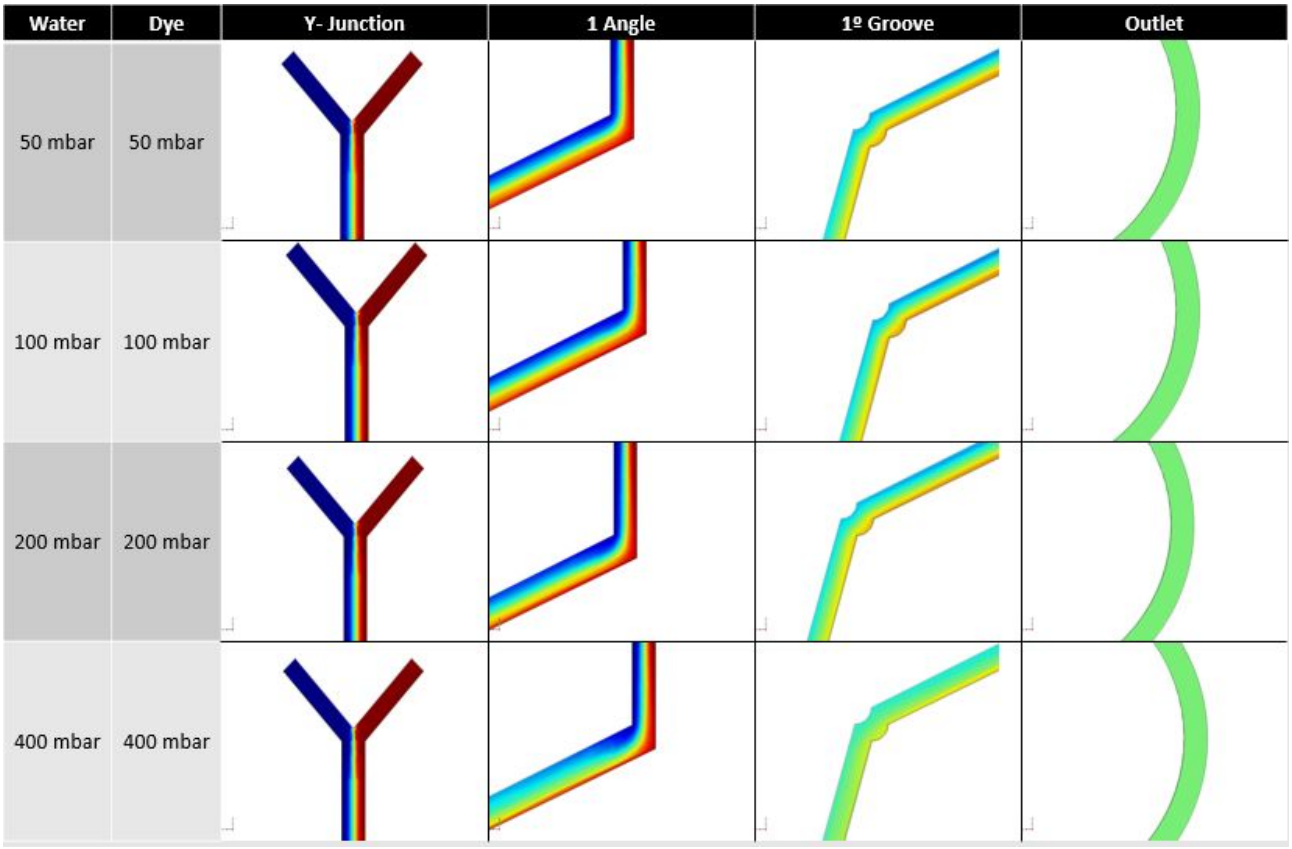

S 1: Numerical study in COMSOL Multiphysics on the influence of pressure on the mixing process. Pressure variation in a range from 50 mbar to 400 mbar. taking into account the mixer input, the first angle, the first groove, and the output of this geometry

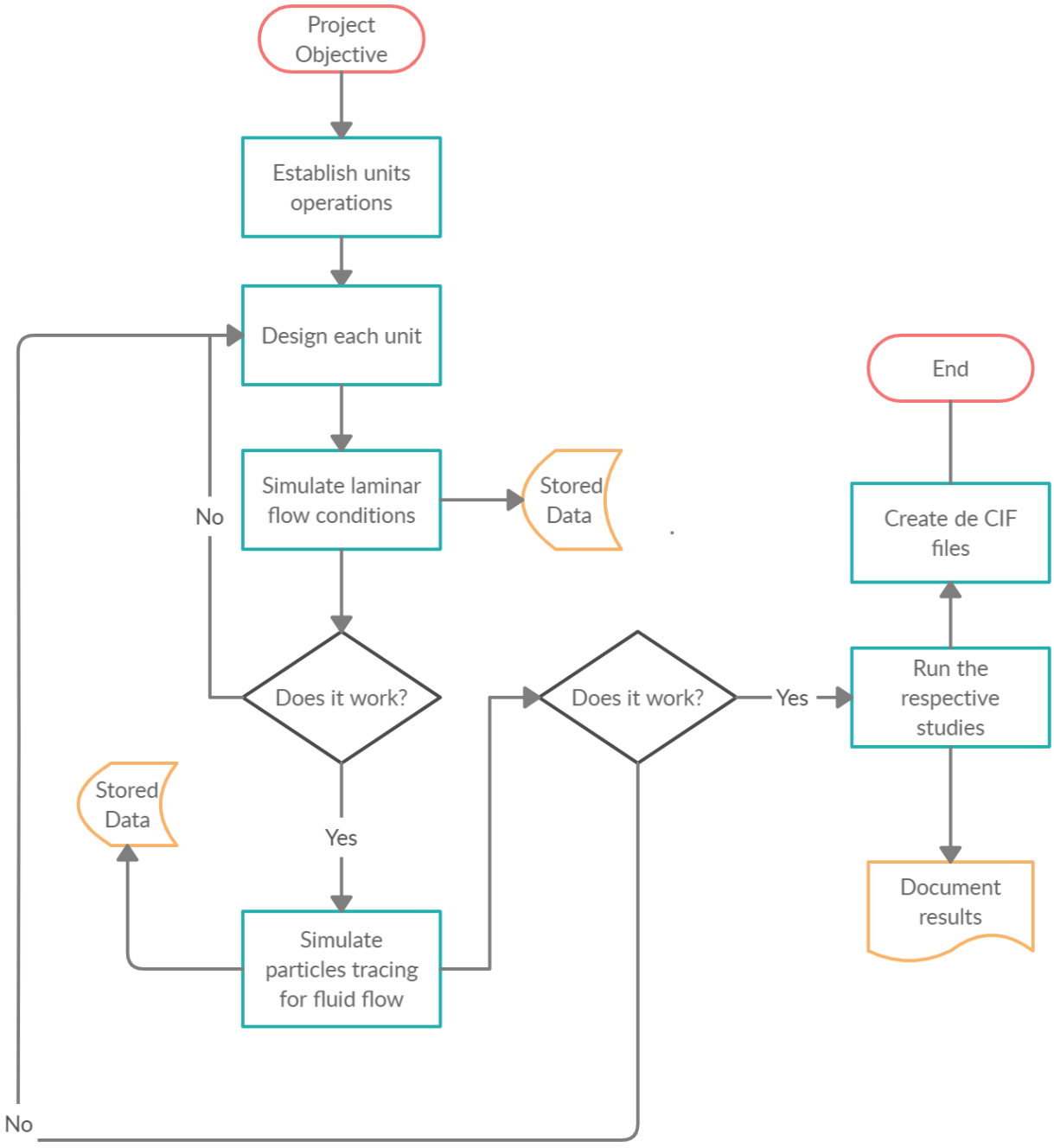

S 2: Flow diagram for the process of creating the geometries, this was implemented in numerical and experimental modeling

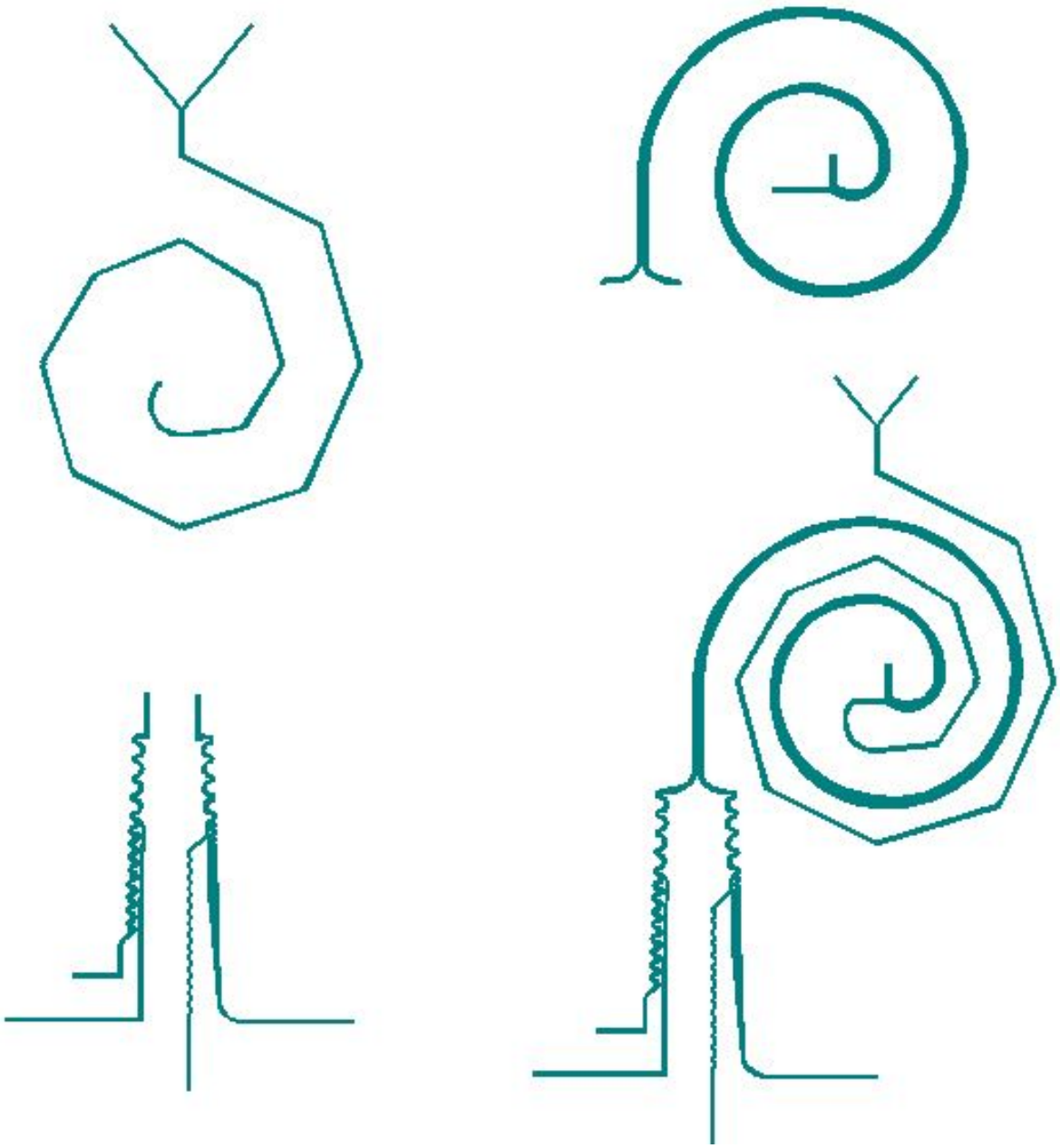

S 3: Geometries established as a result of the design process. These same designs were exported in CIF format to be elaborated on the laser lithography equipment. In addition, these four patterns were elaborated in the same order with PDMS.

	5 μm PS particles		
	Ratio	Pressure [mbar]	Comments
Water inlet	1,2:1	50	Particles leave by both streams
Sample Inlet		42	
Water inlet	1,2:1	100	Particles exit through the outlet of large particles.
Sample Inlet		84	
Water inlet	1,2:1	150	Particles leave by both streams
Sample Inlet		126	
Water inlet	1,2:1	200	The particles exit through the appropriate outlet. minimal amounts take the other outlet
Sample Inlet		168	
Water inlet	1,2:1	250	The particles are in the center of the channel, they exit through both exits
Sample Inlet		210	
Water inlet	1,2:1	300	a stream of particles is created within the fluid they exit through right exit
Sample Inlet		252	
Water inlet	1,2:1	350	a stream of particles is created within the fluid they exit through right exit
Sample Inlet		294	
	20 μm PS particles		
	Ratio	Pressure [mbar]	Comments
Water inlet	1,2:1	50	Particles leave by both streams
Sample Inlet		42	
Water inlet	1,2:1	100	Particles leave by both streams
Sample Inlet		84	
Water inlet	1,2:1	150	Particles leave by both streams
Sample Inlet		126	
Water inlet	1,2:1	200	Particles exit through the outlet of large particles.
Sample Inlet		168	
Water inlet	1,2:1	250	The particles are in the center of the channel, they exit through both exits
Sample Inlet		210	
Water inlet	1,2:1	300	a stream of particles is created within the fluid they exit through left exit
Sample Inlet		252	
Water inlet	1,2:1	350	a stream of particles is created within the fluid they exit through left exit
Sample Inlet		294	

ST 1: Result of the pressure study on the separator, the upper section represents the results obtained and the conditions for the first seven experiments, carried out with particles of 5μm. the lower section are results for the following seven experiments carried out with particles of 20μm